Available online at www.sciencedirect.com
ScienceDirect
Journal of Sound and Vibration 320 (2009) 386–405
JOURNAL OF SOUND AND VIBRATION
www.elsevier.com/locate/jsvi

On the optimal energy harvesting from a vibration source

Jamil M. Renno[a,*], Mohammed F. Daqaq[b], Daniel J. Inman[a]

[a]*Center for Intelligent Material Systems and Structures, Virginia Polytechnic Institute and State University, 310 Durham Hall, Blacksburg, VA 24061-0261, USA*
[b]*Department of Mechanical Engineering, Clemson University, Clemson, SC 29634-0921, USA*

Received 27 October 2007; received in revised form 23 July 2008; accepted 24 July 2008
Handling Editor: S. Bolton
Available online 16 September 2008

Abstract

The optimization of power acquired from a piezoelectric vibration-based energy harvester which utilizes a harvesting circuit employing an inductor and a resistive load is described. The optimization problem is formulated as a nonlinear program wherein the Karush–Kuhn–Tucker (KKT) conditions are stated and the resulting cases are treated. In the first part of the manuscript, the case of a purely resistive circuit is analyzed. While this configuration has received considerable attention in the literature, previous efforts have neglected the effect of damping on the optimal parameters. Here, we explore the impact of damping on power optimality and illustrate its quantitative and qualitative effects. Further, we analyze the effect of electromechanical coupling demonstrating that the harvested power decreases beyond an optimal coupling coefficient. This result challenges previous literature suggesting that higher coupling coefficients always culminate in more efficient energy harvesters. In the second part of this work, the effect of adding an inductor to the circuit is examined. It is demonstrated that the addition of the inductor provides substantial improvement to the performance of the energy harvesting device. It is also shown that within realistic values of the coupling coefficient, the optimal harvested power is independent of the coupling coefficient; a result that supports previous findings for the purely resistive circuit.

1. Introduction

Recent advances in the fields of sensing, computing, and electronics contributed to the development of ultra-small, self-contained, and low-power sensors and actuators. The low-power characteristics of these devices directed a large segment of energy research towards seeking alternative sources to power and maintain them. Recently, an approach based on harvesting ambient vibration energy was proposed. Vibration-based energy harvesters explore the ability of some active materials (e.g., piezoelectric, magnetostrictive, ferroelectric, etc.) to generate an electric potential in response to external mechanical stresses. As a result, these materials can be effectively utilized to transform mechanical strains into useful electrical power. The latter can be stored or used to directly run and maintain low-power devices.

*Corresponding author.
E-mail addresses: renno@vt.edu (J.M. Renno), daqaq@clemson.edu (M.F. Daqaq), dinman@vt.edu (D.J. Inman).
URL: http://www.cimss.vt.edu/inman/index.html (D.J. Inman).

0022-460X/$ - see front matter © 2008 Elsevier Ltd. All rights reserved.
doi:10.1016/j.jsv.2008.07.029

Nomenclature

A	area, m^2
C	capacitance of piezoelectric layer, F
I	current magnitude, A
M	proof mass, kg
M_p	mass of piezoelectric layer, kg
P	magnitude of harvested power, W
R_l	load electric resistance, Ω
V	voltage magnitude, V
X	displacement magnitude, m
c	mechanical modal damping coefficient, N s/m
c_{33}	elasticity coefficient of the piezoelectric layer in the {33} direction, N/m^2
e_{33}	piezoelectric constant in the {33} direction, C/m^2
k	effective stiffness of the harvester, N/m
L	inductance, H
m	approximate effective mass of the harvester, kg
t	thickness, m
v	voltage developed across the electrodes, V
x	piezoelectric layer displacement, m
x_b	base displacement, m
$\bar{\varepsilon}$	mechanical strain, dimensionless
ε_{33}	permittivity of the piezoelectric layer in the {33} direction, F/m
θ	electromechanical coupling coefficient, N/V

Subscript

e	electrode layer property
p	piezoelectric layer property

Superscript

E	property measured at zero electric field
S	property measured at zero strain
T	property measured at zero stress

Many researchers have considered the design and performance optimization of vibration-based energy harvesters [1,2]. For instance, Sodano et al. [3,4] focused on the performance of energy harvesting devices through quantifying the amount of harvested power and the ability to charge storage devices. In other demonstrations, Grisso and Inman [5] proposed an integrated sensor "patch" that can harvest energy from ambient vibrations and temperature gradients. This patch would be able to take measurements and broadcast them when necessary. Rastegar et al. [6] presented a class of efficient energy harvesting devices that are mounted on platforms that vibrate at low frequencies. Priya et al. [7] reported on the advances of powering stationary and mobile untethered sensors using a fusion of energy harvesting approaches. Lefeuvre et al. [8] compared four vibration-powered generators with the purpose of powering standalone systems. They proposed an approach based on processing the voltage generated by the piezoelectric material that would enhance the electromechanical conversion. Badel et al. [9] considered the addition of an electrical switching element in parallel with the piezoelectric element. The switch is triggered at the maxima or minima of the displacement realizing a voltage inversion through an inductor, and hence yielding an increase in the output voltage of the piezoelectric element. Anderson and Sexton [10] presented a model for piezoelectric energy harvesting with a cantilever beam configuration. The model incorporated expressions for variable geometry, tip mass, and material constants.

Researchers such as Roundy [11], Stephen [12], and duToit et al. [13] focused on the optimization of energy harvesters by analyzing the effect of design parameters such as the load resistance and the electromechanical coupling on power optimality. One of the most efficient and simple optimization techniques is based on tuning both of the electrical and mechanical impedances (*impedance matching*). Based on this concept, Wu et al. [14] developed a tunable resonant frequency power harvesting device in the form of a cantilever beam. The device utilized a variable capacitive load to shift the gain curve of the cantilever beam such that it matches the frequency of the external vibration in real time. Twiefel et al. [15] also presented a model that can be tuned to the external excitation frequency. Furthermore, Johnson et al. [16] presented the design of a unimorph piezoelectric cantilever beam tuned to harvest optimal energy from a specific machine application.

Detailed studies on the optimization of energy harvesting devices started with the work of Stephen [12] who assumed that the maximum energy harvesting occurs at the mechanical resonance of the device. duToit and Wardle [17] showed that this assumption hides essential features of the coupled electromechanical response.

They showed that this coupling results in another optimal frequency at the antiresonance. To obtain the complete features of the coupled response, duToit and Wardle [17] used a linearly coupled model to derive an expression for the extracted power. Following similar concepts, Nakano et al. [18] presented a two-port model for electromechanical transducers. They developed a unified method to obtain the optimal conditions for energy harvesting from electromagnetic and piezoelectric transducers.

The purpose of this effort is to provide an analytical understanding of the effects of structural damping and electromechanical coupling on the optimal energy harvesting from a vibration source. Towards that end, we consider a "stack" harvesting device similar to that analyzed in Ref. [17]. However, we propose a harvesting circuit wherein an inductor is employed in parallel or series with the load. Adding an inductor to the harvesting circuit was previously explored by Lesieutre, Ottman, and Hofmann [19] who focused on the analysis of the damping resulting from energy harvesting.

By utilizing the Karush–Kuhn–Tucker (KKT) method [20], we cast the optimization problem as a nonlinear program and examine optimizing the circuit parameters to realize maximum power. Unlike previous research efforts, [17], we account for mechanical damping in the optimality treatment and obtain exact analytical expressions for the optimal frequency ratios as a function of the damping and electromechanical coupling. We demonstrate that neglecting the mechanical damping may result in qualitatively and quantitatively erroneous predictions especially for small quality factors and/or electromechanical coupling coefficients. We also show that there exists an optimal coupling coefficient beyond which the power cannot be increased questioning the previously published idea that a higher coupling coefficient results in higher power values. Results show that the proposed circuit can provide superior performance compared to a purely resistive circuit. In particular, it is shown that at the optimal electric elements, the proposed circuit can harvest maximum power at any excitation frequency.

The remainder of this work is organized as follows. In Section 2 the analytical model of the system under consideration is presented. We first treat the parallel configuration of the inductor and resistor. The optimization problem is stated in Section 3. In Section 4 the harvesting device equipped with a purely resistive circuit is studied. The section presents exact analytical solutions for the optimal frequencies, and presents an analysis of the role of damping and coupling coefficient. In Section 5, we consider the new circuit (parallel configuration). In Section 6, we treat the series configuration of the harvesting circuit. Finally, conclusions for this work are drawn in Section 7.

2. One-dimensional electromechanical analytic model

Fig. 1 displays a stack-type piezoelectric harvesting device with a basic harvesting circuit. We consider the circuit both with and without the inductor. The piezoceramic operates in the {33} mode, and energy is harvested through base excitations.

The equations governing the electromechanical behavior of the system are:

$$m\ddot{x} + c\dot{x} + kx - \theta v = -m\ddot{x}_b, \tag{1}$$

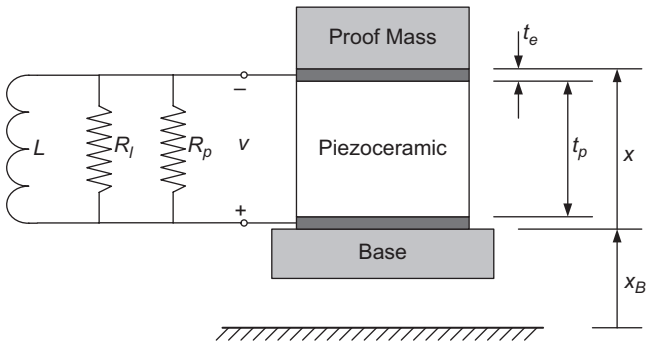

Fig. 1. Schematic of a piezoelectric energy harvester in stack configuration and harvesting circuit.

$$\theta\ddot{x} + C_p\ddot{v} + \frac{1}{R_{eq}}\dot{v} + \frac{1}{L}v = 0, \tag{2}$$

where,

$$m = M + \frac{1}{3}M_p, \quad k = \frac{c_{33}^E A_p}{t_p}, \quad \theta = -\frac{e_{33}A_p}{t_p}, \quad C_p = \frac{\varepsilon_{33}^S A_p}{t_p}. \tag{3}$$

Here, the approximate total mass of the system, m, is taken to be analogous to the effective mass used in a single-degree-of-freedom model of a cantilevered rod with a tip mass in longitudinal vibrations. This approximation has no effect on the analysis presented in this paper, as the system at hand is indeed governed by a single mechanical degree of freedom. A continuum model would certainly present a better approximation of the system dynamics [21,22]. The electrode thickness is neglected ($t_e = 0$) and numerical values of the parameters used in all simulations presented in this paper are listed in Table 1. In the absence of the inductor, Eq. (2) reduces to the model derived in Ref. [17].

In Eq. (2), the equivalent resistance R_{eq} is the parallel resistance of the load and leakage resistances, R_l and R_p, respectively. The leakage resistance, Table 1, is usually much higher than the load resistance [23]. Consequently, in the remainder of this work, we assume $R_{eq} \approx R_l$, and we only refer to the load resistance R_l.

A closed-form analytical solution of the system's displacement and the magnitudes (half-peak-to-peak value) of the voltage developed and the power consumed in the resistive load can be obtained assuming a harmonic base excitation of amplitude X_b and frequency ω. These quantities are presented below normalized with respect to the acceleration amplitude. The normalization choice is motivated by the fact that measurement of acceleration is widely used in experimental settings (e.g. using accelerometers). Hence, the normalized magnitudes are:

$$\left|\frac{X}{\omega^2 X_b}\right| = \frac{1}{\omega_n^2}\frac{\sqrt{\beta^2\Omega^2 + \alpha^2(\beta\Omega^2 - 1)^2}}{\sqrt{B}}, \tag{4}$$

$$\left|\frac{V}{\omega^2 X_b}\right| = \frac{1}{|\theta|}\frac{m\alpha\beta k_e^2\Omega^2}{\sqrt{B}}, \tag{5}$$

$$\left|\frac{P}{(\omega^2 X_b)^2}\right| = \left|\frac{V^2}{R_l(\omega^2 X_b)^2}\right| = \frac{1}{\omega_n^3}\frac{k\alpha\beta^2 k_e^2\Omega^4}{B}, \tag{6}$$

where,

$$B = ((\beta + 2\alpha\zeta)\Omega - \beta(1 + 2\alpha\zeta)\Omega^3)^2 + (\alpha - (2\beta\zeta + \alpha(1 + \beta + \beta k_e^2))\Omega^2 + \alpha\beta\Omega^4)^2, \tag{7}$$

and ω_n is the natural frequency of the mechanical system, α and β are dimensionless time constants, k_e is an alternative electromechanical coupling coefficient, Ω is the frequency ratio, and ζ is the modal damping ratio

Table 1
Data used to simulate the energy harvester

Piezoceramic Harvester's properties	
Proof mass, M (kg)	0.01
Thickness, t_p (m)	0.01
Cross-sectional area, A_p (m^2)	0.0001
Mass, M_p (kg)	0.0075
Permittivity, ε_{33} (F/m)	1.137×10^{-8}
Coupling coefficient, k_{33} (dimensionless)	0.75
Leakage resistance, R_p (Ω)	5×10^9
Base acceleration magnitude	$1g$ ($g = 9.81\,\mathrm{m/s^2}$)

of the mechanical system. These quantities are given below:

$$\omega_n = \sqrt{\frac{k}{m}}, \quad \alpha = R_{\text{eq}}\omega_n C_p\ , \quad \beta = \omega_n^2 L C_p,$$
$$k_e^2 = \frac{\theta^2}{kC_p}, \quad \Omega = \frac{\omega}{\omega_n}, \quad \zeta = \frac{c}{2m\omega_n}. \tag{8}$$

A note regarding the quantity k_e is in order. Throughout this work, k_e will be loosely referred to as the *coupling coefficient*. This quantity is not to be confused with the more traditional coupling coefficient referred to in the literature, k_{33}, given as

$$k_{33}^2 = \frac{d_{33}^2}{s_{33}^E \varepsilon_{33}^T}. \tag{9}$$

Both quantities, k_{33} and k_e, are positive. However, k_{33} is bounded by one, whereas k_e is not. The two coupling coefficients are related through,

$$k_e^2 = \frac{k_{33}^2}{1 - k_{33}^2} = \frac{e_{33}^2}{c_{33}^E \varepsilon_{33}^S}. \tag{10}$$

Lesieutre and Davis [24] provide an interesting discussion on the coupling coefficient of a piezoelectric device and that of its active material.

3. Power optimization

The goal is to maximize the magnitude of the harvested power from the piezoelectric device. In the following, we cast the optimization problem as a nonlinear program with the KKT conditions. The KKT is a generalized form of the long celebrated method of Lagrange multipliers [see for instance Ref. 20]. The objective function to be optimized $\mathscr{P}$, is given by

$$\mathscr{P}(\alpha, \beta) = \frac{1}{\omega_n^3} \frac{k\alpha\beta^2 k_e^2 \Omega^4}{B}. \tag{11}$$

To this end, we desire to obtain optimal values of the resistance and inductance that would achieve maximum power magnitude. Moreover, to obtain meaningful results, the optimal resistance and inductance must be nonnegative. Hence, the nonlinear optimization problem can be stated as follows:

$$\text{Find the } \min_{\alpha,\beta}(-\mathscr{P}) \text{ subject to } g_i(\alpha, \beta) \leqslant 0, \quad i = 1, 2. \tag{12}$$

The negative sign in Eq. (12) indicates that we are seeking a maximum. The constraint functions $g_i(\alpha, \beta)$ declare the nonnegativity of α and β, hence they are given by

$$g_1(\alpha, \beta) = -\alpha \quad \text{and} \quad g_2(\alpha, \beta) = -\beta. \tag{13}$$

The necessary KKT conditions are stated as follows: if the pair $(\alpha_{\text{opt}}, \beta_{\text{opt}})$ is a local optimum, then there exists constants $\mu_i \geqslant 0$ $(i = 1, 2)$, such that

$$-\nabla\mathscr{P}(\alpha_{\text{opt}}, \beta_{\text{opt}}) + \mu^{\text{T}} \cdot \nabla g(\alpha_{\text{opt}}, \beta_{\text{opt}}) = 0 \quad \text{and} \quad \mu_i g_i(\alpha_{\text{opt}}, \beta_{\text{opt}}) = 0 \quad i = 1, 2, \tag{14}$$

where $\nabla\mathscr{P}$ is the gradient of $\mathscr{P}$. Expanding the above expression yields

$$\left.\frac{\partial\mathscr{P}}{\partial\alpha}\right|_{(\alpha_{\text{opt}}, \beta_{\text{opt}})} + \mu_1 = 0 \quad \text{and} \quad \mu_1\alpha_{\text{opt}} = 0 \tag{15a}$$

and

$$\left.\frac{\partial\mathscr{P}}{\partial\beta}\right|_{(\alpha_{\text{opt}}, \beta_{\text{opt}})} + \mu_2 = 0 \quad \text{and} \quad \mu_2\beta_{\text{opt}} = 0. \tag{15b}$$

Moreover, the KKT necessary conditions state that if the sufficient conditions, Eqs. (15a,b), are satisfied, and $\mathscr{P}(\alpha,\beta)$ and $g_i(\alpha,\beta)$ are convex functions, then the pair $(\alpha_{\text{opt}},\beta_{\text{opt}})$ is a global optimum. The constraint functions $g_i(\alpha,\beta)$ are convex by construction. Moreover, one can obtain the Hessian of $\mathscr{P}(\alpha,\beta)$ and show that it is positive definite. Hence, an optimal pair $(\alpha_{\text{opt}},\beta_{\text{opt}})$ is a global optimum.

The resulting system of equalities and inequalities requires thorough analysis to obtain the possible optimal solutions $(\alpha_{\text{opt}},\beta_{\text{opt}})$. A preliminary investigation reveals the existence of the following cases:

(a) *Case* I: If $\mu_1\neq 0$ and $\mu_2\neq 0$, then $\alpha_{\text{opt}}=\beta_{\text{opt}}=0$ as per Eqs. (15a,b). This result violates the purpose of the problem, as no power can be extracted in the absence of an electric circuit.

(b) *Case* II: If $\mu_1\neq 0$ and $\mu_2=0$, then α_{opt} must be zero, and we have to solve the following system:

$$\left.\frac{\partial\mathscr{P}}{\partial\alpha}\right|_{(0,\beta_{\text{opt}})}=0 \quad \text{and} \quad \left.\frac{\partial\mathscr{P}}{\partial\beta}\right|_{(0,\beta_{\text{opt}})}=0. \tag{16}$$

An optimal value β_{opt} can be obtained, however, the solution is not useful. The power is consumed by the resistor, and since $\alpha_{\text{opt}}=0$, the suggestion is that we are harvesting power with an infinite magnitude which is not realistic.

(c) *Case* III: This case occurs if $\mu_1=0$ and $\mu_2\neq 0$. This yields the purely resistive circuit which was analyzed in the literature. The optimization problem reduces to solving the following equation:

$$\left.\frac{\partial\mathscr{P}}{\partial\alpha}\right|_{\alpha_{\text{opt}}}=0. \tag{17}$$

duToit and Wardle [17] solved this equation in the absence of mechanical damping. Here, we extend their results by including the effect of damping.

(d) *Case* IV: When $\mu_1=0$ and $\mu_2=0$, then $\alpha_{\text{opt}}\neq 0$ and $\beta_{\text{opt}}\neq 0$. As such, Eqs. (15a,b) reduce to solving the following nonlinear system:

$$\left.\frac{\partial\mathscr{P}}{\partial\alpha}\right|_{(\alpha_{opt},\beta_{\text{opt}})}=0 \quad \text{and} \quad \left.\frac{\partial\mathscr{P}}{\partial\beta}\right|_{(\alpha_{opt},\beta_{\text{opt}})}=0. \tag{18}$$

This case represents a separable optimization problem and will be analyzed in Section 5.

4. Analysis of Case III

To solve the optimization problem posed in Eq. (17), duToit and Wardle [17] among others [12,14] set the damping ratio, ζ, to zero. Then, they analyzed the harvesting circuit at short- and open-circuit conditions by letting the dimensionless time constant α approach zero and infinity, respectively, to obtain two optimal frequency ratios (for which the power is maximum). These two frequency ratios were denoted as the resonance frequency, Ω_r, and the antiresonance frequency, Ω_{ar}, given by

$$\Omega_r=1 \quad \text{and} \quad \Omega_{\text{ar}}=\sqrt{1+k_e^2}. \tag{19}$$

At zero damping ratio, the preceding expressions accurately describe the optimal frequency ratios for which the power harvested is indeed maximum. However, this result suggests that the optimal frequency ratios are invariant to changes in the damping ratio. Towards that end, we solve Eq. (17) and obtain the value of α_{opt} as

$$\alpha_{\text{opt}}^2=\frac{1}{\Omega^2}\frac{(1-\Omega^2)^2+(2\zeta\Omega)^2}{([1+k_e^2]-\Omega^2)^2+(2\zeta\Omega)^2}. \tag{20}$$

Next, we optimize the frequency ratio. We substitute Eq. (20) in Eq. (6), set the derivative of the resulting power expression to zero, and solve the resulting equation for Ω. The resulting polynomial is of the 12th degree in Ω and obtaining analytical expressions for all the roots of this polynomial is rather a formidable task. Consequently, we resort to plotting the numerical solutions of the resulting equation versus the damping ratio, ζ, at a given coupling coefficient k_e, as displayed in Fig. 2.

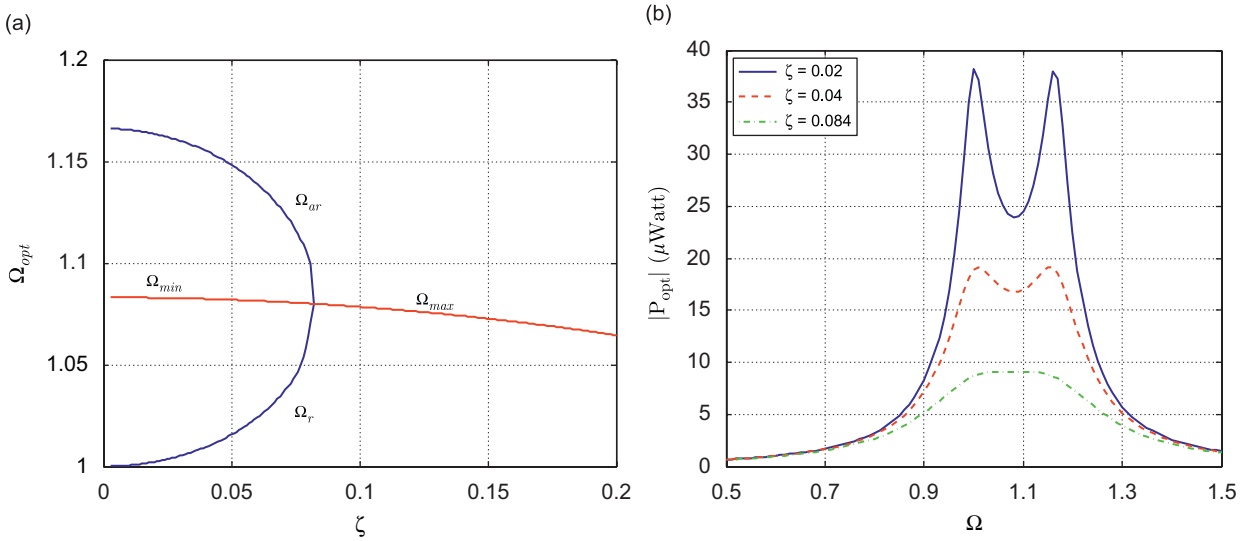

Fig. 2. Optimal frequency ratios and harvested power at $\kappa = 0.6$ and corresponding α_{opt}: (a) variation of optimal frequency ratios with the damping ratio ζ and (b) magnitude of optimal harvested power at different damping ratios, ζ.

At $\zeta = 0$, the system has three real positive extrema: two maxima and a minimum. The maxima are $\Omega_r = 1$ and $\Omega_{ar} = \sqrt{1 + k_e^2}$ as predicted in Ref. [17]. The third root is a minimum, given as

$$\Omega_{min} = \frac{1}{\sqrt{6}} \sqrt{2 + k_e^2 + \sqrt{16 + 16k_e^2 + k_e^4}}. \tag{21}$$

Examining Fig. 2a, we observe that as the damping ratio increases, the value of Ω_r increases whereas the value of Ω_{ar} decreases. On the other hand, the value of the minimum, Ω_{min} decreases slowly relative to changing values of ζ. The variation of these three roots resembles a subcritical pitchfork bifurcation with the damping ratio being the bifurcation parameter. More specifically, for damping ratios that are less than a particular damping ratio (*bifurcation damping ratio* ζ_b), the optimal power resembles a double-peak single-well potential function with the double peaks representing the two maxima and the well representing the minima, Fig. 2b. At ζ_b, the power expression becomes of the single-peak potential type and the values of the three extrema become a single maximum. This solution is an extension of the minimum solution prior to crossing ζ_b. Further increase in ζ beyond ζ_b results in a decrease in the optimal frequency ratio. For the case considered here, the bifurcation damping ratio was found to be $\zeta_b = 0.084$.

The associated magnitudes of the voltage and displacement are displayed in Fig. 3a and b, respectively. Fig. 4a displays the magnitude of the current passing through R_l. It is worth noting that, at the resonance frequency ratio, Ω_r, the current magnitude is at a maximum whereas the voltage magnitude is at a minimum. Hence, Ω_r is a suitable operating point for applications requiring high current, such as charging a storage device. This observation is reversed at the antiresonance frequency ratio, Ω_{ar}, where the voltage is at a maximum and the current is at a minimum. This operating condition is suitable for applications requiring high voltage, such as wireless sensors, which mainly use diodes and transistors. Furthermore, the optimal value of the displacement behaves similar to the voltage. It assumes a small value at the resonance frequency, Fig. 4b. Recall that the time constant α is proportional to the load resistance, R_l. However, the power is inversely proportional to the load resistance. Hence, to maintain the same harvested power, the voltage and the resistance have to behave similarly. The magnitude of the voltage and R_l are both small at Ω_r and both attain maxima at Ω_{ar}.

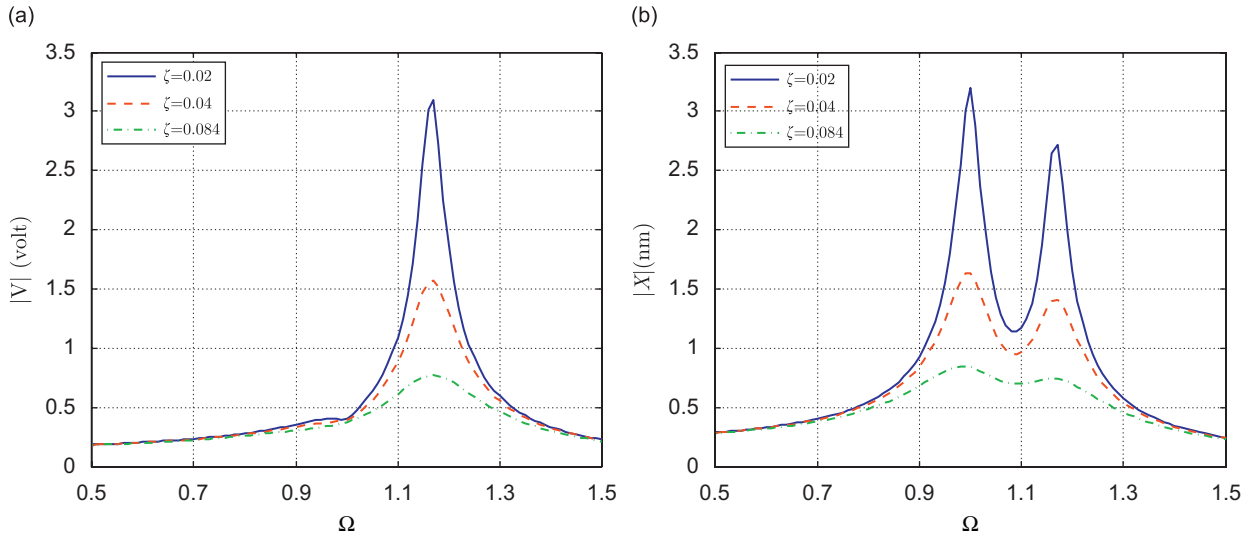

Fig. 3. Optimal voltage and displacement magnitudes at different damping ratios with $\kappa = 0.6$: (a) optimal voltage magnitude vs. frequency ratio and (b) optimal displacement magnitude vs. frequency ratio.

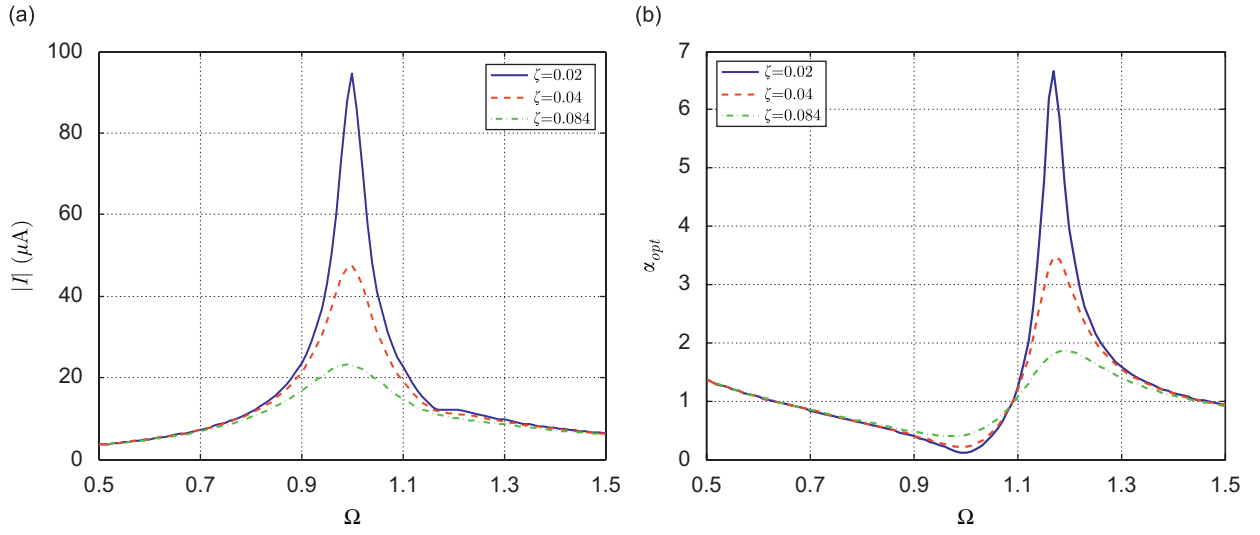

Fig. 4. Optimal current magnitude and optimal time constant α at different damping ratios with $\kappa = 0.6$: (a) current magnitude vs. frequency ratio and (b) α_{opt} vs. frequency ratio.

4.1. Exact solution for optimal frequencies

Using the numerical bifurcation diagram of Fig. 2, exact analytical expressions for the resonance, Ω_r, and antiresonance, Ω_{ar}, frequency ratios can be obtained through a trial and error process. These roots are:

$$\Omega_r = \frac{\sqrt{2 - 4\zeta^2 + k_e^2 - \sqrt{16\zeta^4 - 16\zeta^2 - 8\zeta^2 k_e^2 + k_e^4}}}{\sqrt{2}}, \tag{22}$$

$$\Omega_{\mathrm{ar}} = \frac{\sqrt{2 - 4\zeta^2 + k_e^2 + \sqrt{16\zeta^4 - 16\zeta^2 - 8\zeta^2 k_e^2 + k_e^4}}}{\sqrt{2}}. \tag{23}$$

The exact solution for $\Omega_{\max}$ which represents the middle branch of the bifurcation diagram displayed in Fig. 2 is found next. Recall that Eq. (23) yields complex quantities when $\zeta > \zeta_b$. This can be exploited to solve for $\Omega_{\max}$, since the two roots obtained so far, Ω_r and Ω_{ar} constitute four roots as the conjugate of a complex root is also a root. Moreover, the opposite of these roots and their conjugates are also roots. Hence, by eliminating these eight roots, one can solve a polynomial of the 4th degree instead of solving a polynomial of the 12th degree. The root presenting the middle branch is,

$$\Omega_{\min} = \frac{\sqrt{6}\sqrt{2 - 4\zeta^2 + k_e^2 + \sqrt{16 + 16\zeta^4 + 16k_e^2 + k_e^4 - 8\zeta^2(2 + k_e^2)}}}{6}. \tag{24}$$

Now, further analysis can be conducted to expand our understanding of optimal energy harvesters.

4.2. Criticality treatment

The expressions for Ω_r and Ω_{ar} are new and warrant some investigation. For instance, note that these quantities are complex when,

$$16\zeta^4 - 16\zeta^2 - 8\zeta^2 k_e^2 + k_e^4 < 0. \tag{25}$$

Inequality (25) can be solved to yield exact values of the bifurcation damping ratio discussed above as well as a bifurcation coupling coefficient,

$$\zeta_b = \tfrac{1}{2}\left(-1 + \sqrt{1 + k_e^2}\right), \tag{26}$$

$$(k_e)_b = 2\sqrt{\zeta + \zeta^2}. \tag{27}$$

4.2.1. Effects of the bifurcation damping ratio

Eq. (26) reveals that the bifurcation damping ratio is independent of the harvesting circuit parameters. Furthermore, the bifurcation damping ratio is only a function of the coupling coefficient k_e, and hence depends only on the properties of the piezoelectric material used. As k_e approaches zero, ζ_b approaches zero, and the transition bifurcation takes place at lower values of ζ. On the other hand, as the coupling coefficient increases, the bifurcation damping increases. In other words, the two branches of Ω_r and Ω_{ar} coexist for larger values of the damping ratio, Fig. 5a. This is favorable as the existence of the two branches provides an operating point, Ω_r for low voltage/high current, and another operating point, Ω_{ar}, for high voltage/low current as discussed earlier.

A key point here is that if the mechanical damping is neglected when optimizing the frequency ratio, then erroneous values of frequency ratios, time constant and optimal load resistance result. Fig. 5b shows variation of the optimal time constant α_{opt} with the damping ratio ζ at $k_e = 0.6$. As predicted earlier by duToit and Wardle [17], for $\zeta = 0$, short circuit condition ($R_l = 0$) maximizes the power at resonance whereas open circuit condition ($R_l \to \infty$) maximizes the power at antiresonance. However, as ζ is increased, the optimal time constant obtained by duToit and Wardle [17] deviates from the actual values. More importantly, for values of ζ beyond ζ_b, the previously published model predicts that two values of R_l maximize the power. However, for damping ratios beyond ζ_b, there is only one value for R_l that maximizes the power. This value can be obtained analytically by substituting the solution of the optimal frequency ratio for $\zeta > \zeta_b$, Eq. (24), in the expression determined for the optimal time constant α_{opt}, Eq. (20). The optimal resistance values can then be obtained.

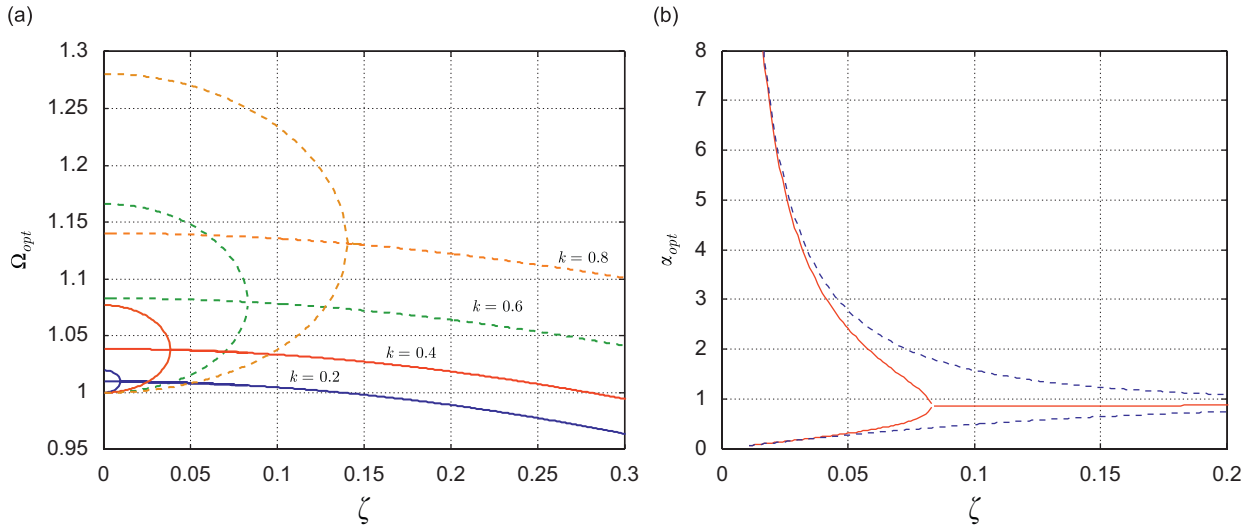

Fig. 5. The bifurcation diagram at different coupling value and the effect of the bifurcation on the optimal time constant: (a) bifurcation diagrams of the optimal frequency ratios vs. the damping ratio ζ for different values of κ and (b) variation of the optimal time constant α_{opt} with the damping ratio ζ at $\kappa = 0.6$. The solid line is the optimal time constant calculated with damping included, whereas the dashed line results if the formulation of duToit and Wardle [17] is used.

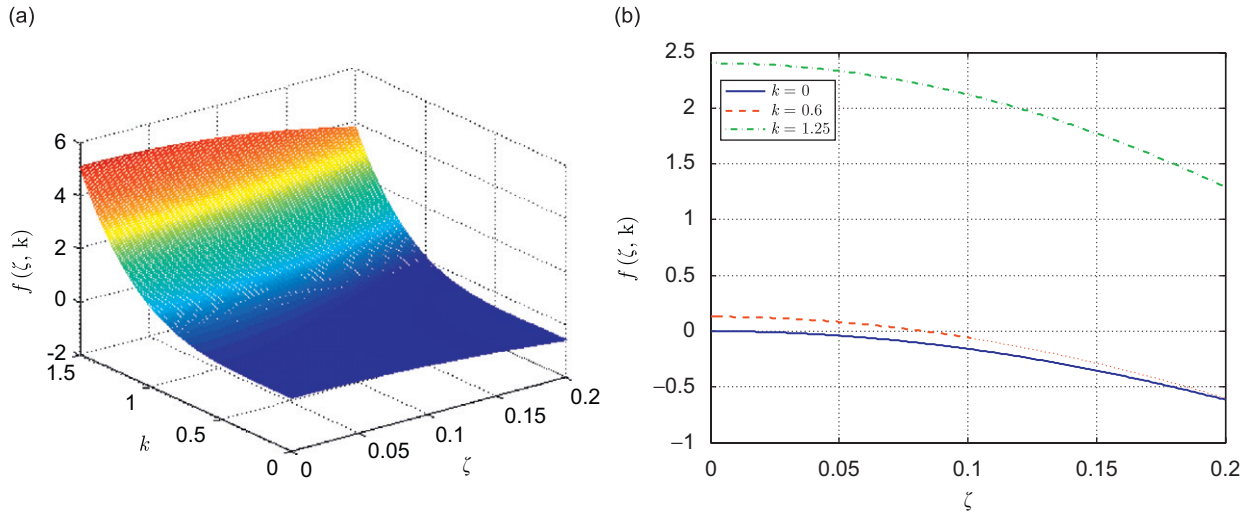

Fig. 6. Studying the criticality issues: (a) three-dimensional display of the function $f(\zeta, \kappa)$ and (b) $f(\zeta, \kappa)$ vs. ζ for constant values of κ.

4.2.2. *Effects of the bifurcation coupling coefficient*

To further understand the effects of the bifurcation coupling coefficient, inequality (25) should be studied more. As such, we define

$$f(\zeta, k_e) = 16\zeta^4 - 16\zeta^2 - 8\zeta^2 k_e^2 + k_e^4. \tag{28}$$

Fig. 6a displays the behavior of this function with varying values of ζ and k_e. As ζ is increased for constant values of k_e, $f(\zeta, k_e)$ varies from being large and positive to being small and negative. This behavior is shown in Fig. 6b, and was also demonstrated in Fig. 5a. This situation gives rise to two operating points that produce

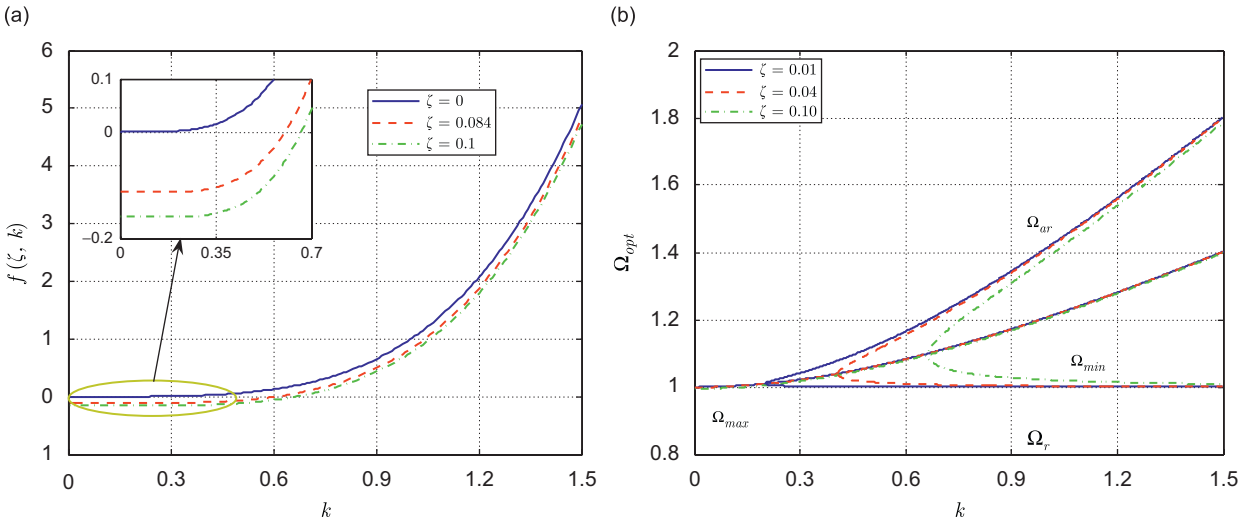

Fig. 7. Effect of ζ on $f(\zeta,\kappa)$ and the resonance and antiresonance frequencies: (a) $f(\zeta,\kappa)$ vs. ζ for constant values of κ and (b) bifurcation diagrams of the optimal frequency ratios vs. the coupling coefficient κ for different values of ζ.

the same amount of power; one provides high voltage/low current, and the other provides high current/low voltage.

On the other hand, for constant ζ values, $f(\zeta,k_e)$ is negative for small values of the coupling coefficient and becomes positive when the coupling coefficient crosses the bifurcation coupling coefficient, $(k_e)_b$. This behavior can be concluded from Fig. 7a and indicates the existence of another bifurcation diagram that is "opposite" to the one obtained previously. It turns out that, for small values of k_e, a single maximum exists. Beyond the value of $(k_e)_b$, this maximum becomes a minimum, and two roots branch out. These two branches represent two maxima.

Eqs. (23) and (24) can be used to study the behavior of the optimal frequency ratios for varying values of k_e. This behavior is illustrated in Fig. 7b, where the bifurcation diagram presenting the optimal frequency ratios is shown for different values of the damping ratio. We note that for all the values of damping ratio used, all the branches of the bifurcation diagram coincide for high values of the coupling coefficient. Moreover, the middle branches ($\Omega_{\max}$ before $(k_e)_b$, $\Omega_{\min}$ after $(k_e)_b$) differ slightly before $(k_e)_b$, and practically coincide after crossing $(k_e)_b$. Additionally, the bifurcation coupling coefficient increases as the damping increases, which is also evident from Eq. (27).

4.3. Electromechanical coupling

In order to gain a better understanding of the effect of the electromechanical coupling coefficient, k_e, on the power harvested, we use Eq. (2) to relate the power harvested to the displacement of the stack,

$$|P| = \frac{k\alpha k_e^2 \Omega^2 \omega_n}{1+\alpha^2\Omega^2}|X|^2. \tag{29}$$

Eq. (29) states that for a constant Ω, α, and $|X|$, the harvested power increases as k_e increases. However, although Ω and α can be maintained constant, it is almost impossible to maintain the displacement magnitude $|X|$ constant. More specifically, Eq. (4) indicates that for constant input acceleration amplitude, as k_e increases, the displacement magnitude $|X|$ decreases. Therefore, for constant input acceleration amplitude, an increase in k_e is not necessarily accompanied by an increase in the harvested power.

Furthermore, according to Eq. (4), as k_e approaches zero, $|X|$ is maximized, therefore all the energy supplied by the environment is transferred to the structure. However, this energy cannot be harvested as per Eq. (6).

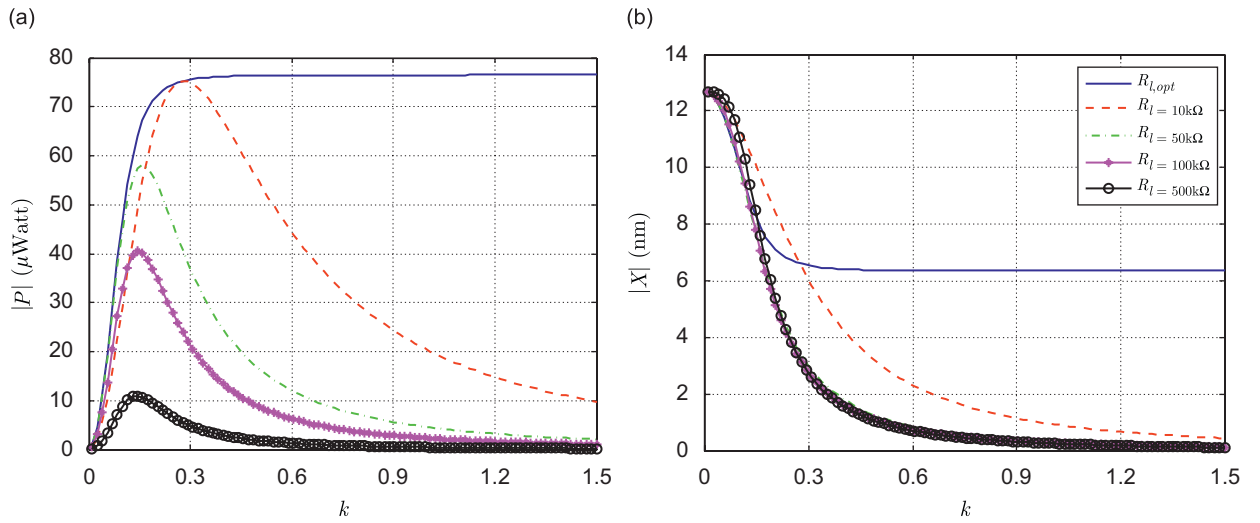

Fig. 8. Variation of the power and displacement with the coupling coefficient for different values of load resistance, R_l, at $\Omega = \Omega_r$ and $\zeta = 0.01$: (a) harvested power vs. coupling coefficient and (b) displacement vs. coupling coefficient.

The above discussion suggests that a larger k_e does not always imply a more efficient energy harvester. The coupling coefficient k_e also acts as a damping term that minimizes the flow of energy from the environment to the harvesting device. For a given frequency ratio and time constant, Ω and α, the optimal coupling coefficient can be obtained as

$$(k_e)^2_{\text{opt}} = \frac{1}{\alpha\Omega}\sqrt{(1+\alpha^2\Omega^2)(1+(4\zeta^2-2)\Omega^2+\Omega^4)}. \tag{30}$$

Note that Eq. (30) has a solution for all possible values of α, Ω, and ζ. For $\zeta = 0$, $\Omega = \Omega_r = 1$ as per Eq. (23). Then, the optimal coupling coefficient, $(k_e)_{\text{opt}} = 0$ and the harvested power approaches infinity according to Eq. (6). This is counterintuitive, physically unrealizable, and can be explained by the fact that the displacement amplitude $|X|$ unrealistically approaches infinity at resonance for zero damping ratio and zero coupling coefficient.

Fig. 8a shows the variation of the harvested power with the coupling coefficient for different values of load resistance at the resonance frequency with $\zeta = 0.01$. For a given R_l, as the coupling coefficient increases, the harvested power increases until it reaches a maximum value at $(k_e)_{\text{opt}}$. Further increase in k_e results in a decrease in the harvested power which approaches zero as the coupling coefficient increases.

At the optimal load resistance, $R_{l,\text{opt}}$, the harvested power saturates at the optimal coupling coefficient, $(k_e)_{\text{opt}}$. Moreover, the displacement reaches a *final* value as well, Fig. 8b. These results might be counterintuitive, yet they are supported by the equations governing the behavior of the system. Replace the expression of the optimal time constant, Eq. (20), in the expression of the displacement and power magnitudes, Eqs. (4) and (6). Then, compute the limit of these expressions as k_e approaches infinity,

$$|P_{k_e\to\infty}| = \frac{k\Omega}{2(2\zeta\Omega+\sqrt{1+(4\zeta^2-2)\Omega^2+\Omega^4})\omega_n^3}, \tag{31}$$

$$|X_{k_e\to\infty}| = \frac{1}{\omega_n^2\sqrt{2+2\Omega((4\zeta^2-2)\Omega+\Omega^3+2\zeta\sqrt{1+(4\zeta^2-2)\Omega^2+\Omega^4}}}. \tag{32}$$

The values in Eqs. (31) and (32) can be used to verify the saturation limits displayed in Figs. 8a and b.

5. Analysis of Case IV

For Case IV, we solve Eq. (18) which yields the following optimal values for α and β:

$$\alpha_{\text{opt}} = \frac{\Omega^4 + (4\zeta^2 - 2)\Omega^2 + 1}{2\zeta k_e^2 \Omega^2} \tag{33a}$$

and

$$\beta_{\text{opt}}^{(1)} = 0 \geqslant 0 \quad \text{and} \quad \beta_{\text{opt}}^{(2)} = \frac{\Omega^4 + (4\zeta^2 - 2)\Omega^2 + 1}{\Omega^2(\Omega^4 - (2 + k_e^2 - 4\zeta^2)\Omega^2 + k_e^2 + 1)} \geqslant 0. \tag{33b}$$

Note that α_{opt} is independent of β_{opt} and that there are two solutions for β_{opt}. The first solution, $\beta_{\text{opt}}^{(1)}$, implies that no inductor is added to the circuit. Section 4 treated this case in detail. The second solution, $\beta_{\text{opt}}^{(2)}$, reveals interesting results and requires further attention. For instance, while the first solution obtained, $\beta_{\text{opt}}^{(1)}$, always satisfies the constraint $\beta_{\text{opt}} \geqslant 0$, the second solution $\beta_{\text{opt}}^{(2)}$ is less than zero when

$$\Omega_1 < \Omega < \Omega_2 \quad \text{and} \quad \zeta \leqslant \zeta_b, \tag{34}$$

where

$$\Omega_1 = \frac{\sqrt{2 - 4\zeta^2 + k_e^2 - \sqrt{16\zeta^4 - 16\zeta^2 - 8\zeta^2 k_e^2 + k_e^4}}}{\sqrt{2}},$$
$$\Omega_2 = \frac{\sqrt{2 - 4\zeta^2 + k_e^2 + \sqrt{16\zeta^4 - 16\zeta^2 - 8\zeta^2 k_e^2 + k_e^4}}}{\sqrt{2}}. \tag{35}$$

The resulting values of Ω_1 and Ω_2 are the resonance and antiresonance frequency ratios obtained in Eq. (23). Hence, $\beta_{\text{opt}}^{(1)}$ optimizes the system, always satisfies the KKT conditions, and was treated in Section 4. However, $\beta_{\text{opt}}^{(2)}$ violates the KKT conditions when $\Omega_1 \leqslant \Omega \leqslant \Omega_2$ and $\zeta \leqslant \zeta_b$, and in such circumstance, the first optimal value $\beta_{\text{opt}}^{(1)}$ is used.

Through the rest of this work, β_{opt} will refer solely to $\beta_{\text{opt}}^{(2)}$ unless specified otherwise. It is worth noting that β_{opt} is independent of α_{opt}. In other words, the optimization problem at hand is of an additive (separable) nature. The power can be independently optimized with respect to each electrical element. Based on these findings, an optimal power expression can be obtained by substituting α_{opt} and β_{opt} in Eq. (6), yielding

$$\mathscr{P}_{\text{opt}} = \frac{k}{8\zeta\omega_n^3}. \tag{36}$$

Observing Eq. (36), we can state the following:

(a) The optimal power is independent of the coupling coefficient k_e. It was shown in Section 4 that at the optimal resistance of the purely resistive energy harvesting circuit, the power saturates and does not increase as k_e increases. The result obtained here is in agreement with the previous findings. However, Eq. (36) suggest that the harvested power would remain constant even if the coupling coefficient k_e becomes arbitrarily small or arbitrarily large. To investigate this, we examine the expressions of the optimal voltage and current,

$$\left|\frac{V_{\text{opt}}}{\omega^2 X_b}\right| = \frac{k\sqrt{C}(1 + k_e^2 - (2 + k_e^2 - 4\zeta^2)\Omega^2 + \Omega^4)}{4C_p\zeta k_e(1 + (4\zeta^2 - 2)\Omega^2 + \Omega^4)\omega_n^2}, \tag{37a}$$

$$\left|\frac{I_{\text{opt}}}{\omega^2 X_b}\right| = \frac{C_p k_e(1 + (4\zeta^2 - 2)\Omega^2 + \Omega^4)}{2\sqrt{C}(1 + k_e^2 - (2 + k_e^2 - 4\zeta^2)\Omega^2 + \Omega^4)\omega_n}, \tag{37b}$$

where,

$$C = \frac{C_p(1 + (4\zeta^2 - 2)\Omega^2 + \Omega^4)^3}{k\Omega^2(1 + k_e^2 - (k_e^2 - 4\zeta^2 + 2)\Omega^2 + \Omega^4)^2}. \tag{37c}$$

Examining Eq. (37c) shows that

$$\lim_{k_e \to 0} |V_{\text{opt}}| = \infty \quad \text{and} \quad \lim_{k_e \to 0} |I_{\text{opt}}| = 0, \tag{38a}$$

however

$$\lim_{k_e \to \infty} |V_{\text{opt}}| = 0 \quad \text{and} \quad \lim_{k_e \to \infty} |I_{\text{opt}}| = \infty. \tag{38b}$$

Eq. (38b) removes any potential confusion, and show that Eq. (36) is only valid for realistic values of k_e. For very small (or very large) values of k_e, the voltage and current values are not useful.

(b) The optimal power is independent of the frequency ratio. Previous works concluded that maximum power can be achieved at the resonance frequency [12]. This concept was advanced in a later work [17], where it was shown that two frequency ratios, resonance and antiresonance, maximize the value of the harvested power. However, the optimal power of Eq. (36) is independent of the frequency ratio, suggesting that the device harvests the same maximum power at any frequency ratio.

Another notion is realized by deriving the expression for the optimal strain rate within the piezoelectric element. This can be obtained by calculating the magnitude of $\dot{\bar{\varepsilon}} = \dot{x}/t_p$, and substituting the optimal circuit elements values α_{opt} and β_{opt} which simplifies to

$$\left|\frac{\dot{\bar{\varepsilon}}}{\omega^2 X_b}\right| = \frac{1}{4t_p\zeta\omega_n}. \tag{39}$$

The above expression implies that, for constant base acceleration, to achieve optimal power everywhere in the frequency domain, the harvesting device has to maintain a constant optimal strain-rate.

5.1. Discussion and analysis of Case IV

The optimization results presented above deserve further analysis. First, it is worth noting that the optimal power expression in Eq. (36) is the same approximate expression obtained for a purely resistive circuit at the

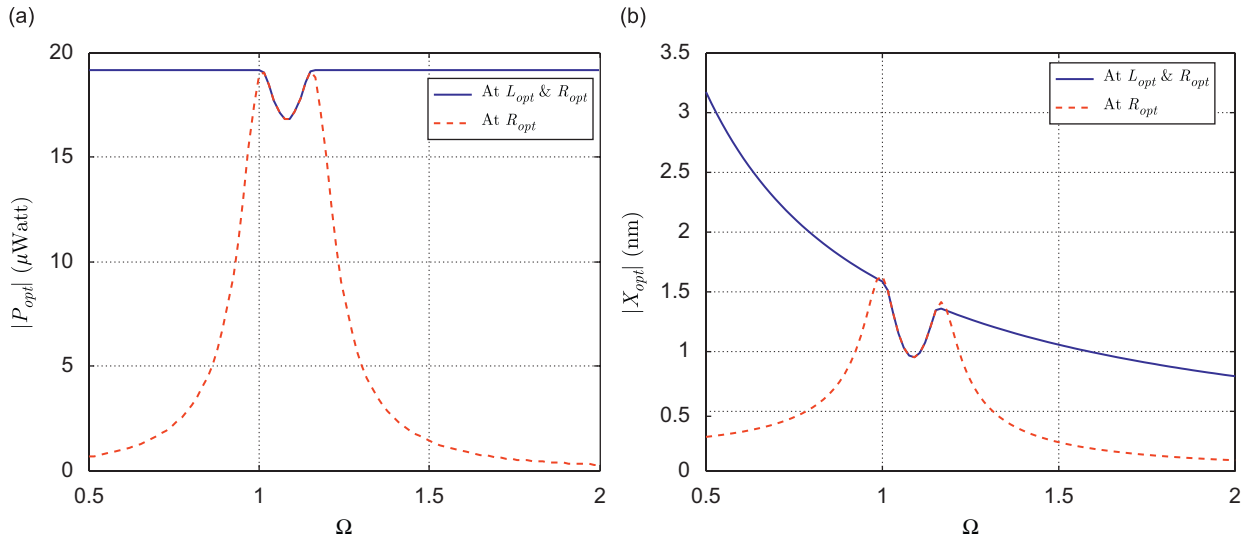

Fig. 9. Optimal power and displacement at $\kappa = 0.6$ and $\zeta = 0.04 < \zeta_b$ (inductor in parallel): (a) optimal harvested power and (b) optimal displacement.

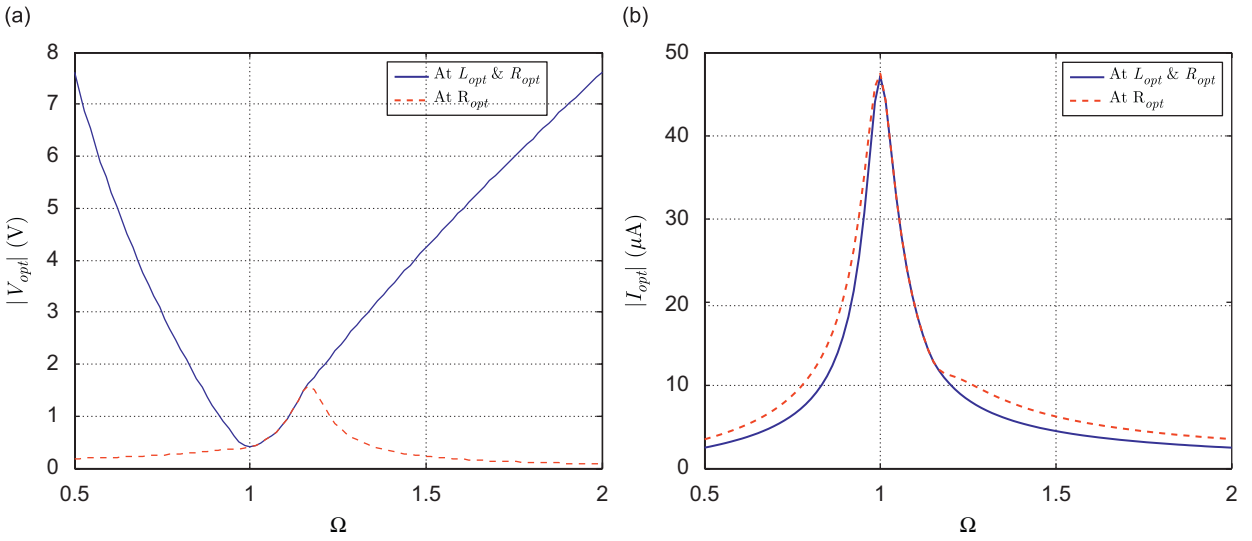

Fig. 10. Optimal voltage and current at $\kappa = 0.6$ and $\zeta = 0.04 < \zeta_b$ (inductor in parallel): (a) optimal voltage and (b) optimal current.

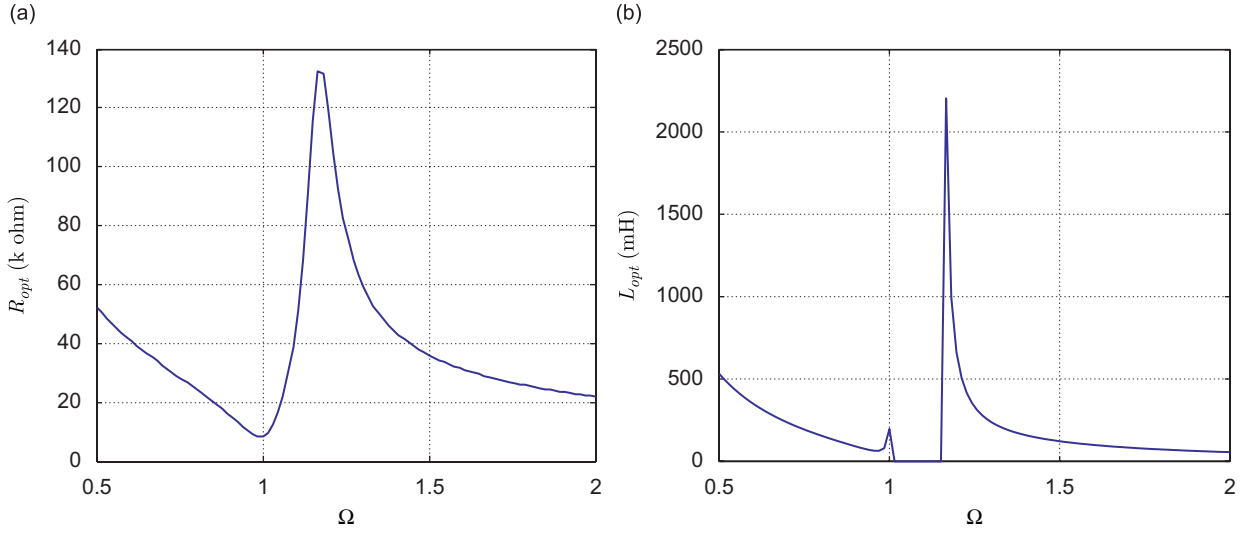

Fig. 11. Optimal resistance and inductance at $\kappa = 0.6$ and $\zeta = 0.04 < \zeta_b$ (inductor in parallel): (a) optimal resistance and (b) optimal inductance.

resonance and antiresonance frequency ratios for small values of (ζ/k_e). This is clearly demonstrated in Fig. 9a. However, for Case IV, Eq. (36) is valid for all frequency ratios and any value of (ζ/k_e) provided that $\beta_{\text{opt}} > 0$. This implies that, by optimizing the inductor and resistor of the energy harvesting circuit, one can harvest the maximum power everywhere in the frequency domain making the proposed circuit superior to that utilized previously in Ref. [17] among others.

Fig. 9a displays the optimal power at a coupling coefficient, $k_e = 0.6$, and a damping ratio $\zeta = 0.04 < \zeta_b = 0.085$. The presence of the inductor helps transform the power figure of Fig. 8a into a broadband-constant curve as shown in Fig. 9a. Fig. 10a and b display the voltage and current. It is worth noting that, the power, voltage, and current coincide with those obtained for Case III when $\Omega_r < \Omega < \Omega_{\text{ar}}$ ($\beta_{\text{opt}} = 0$). To further examine the practicality of the optimal results, one has to check the values obtained for the optimal resistance and inductance. As illustrated in Fig. 11a and b, these values are for the most part

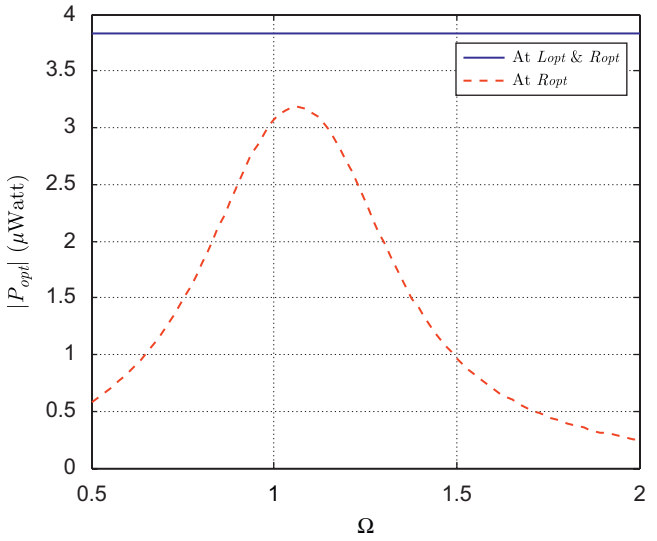

Fig. 12. Optimal power at $\kappa = 0.6$ and $\zeta = 0.2 > \zeta_b$ (inductor in parallel).

practical quantities that can be found off the shelf or even manufactured, if needed. For instance, at $\Omega = 2$, the optimal values for the load resistance and inductance are, respectively, 22 kΩ and 55 mH which are achievable values. It is worth noting that, near the antiresonance and for very small excitation frequencies, the optimal inductance can be rather large.

Fig. 12 shows the optimal power with the same coupling coefficient used previously ($k_e = 0.6$) and a damping ratio $\zeta = 0.2 > \zeta_b$. A constant optimal power can still be harvested if optimal circuit elements are used, as per Eq. (36). Moreover, the power harvested via the proposed circuit is higher than the maximum power that can be obtained via the circuit utilized in Ref. [17]. It is also worth noting that the expression of Eq. (36) cannot describe the optimal power harvested using the purely resistive circuit as the ratio (ζ/k_e) is not small any more.

6. Placing the inductor in series

For the purpose of completion and comparison, we consider in this section, the optimization problem when the inductor is connected in series with the resistor. In this case, the governing equations are:

$$m\ddot{x} + c\dot{x} + kx - \theta(\dot{q}R_{\text{eq}} + \ddot{q}L) = -m\ddot{x}_b, \tag{40}$$

$$C_pL\ddot{q} + C_pR_{\text{eq}}\dot{q} + q\theta x = 0 \quad \text{where } i = \frac{\mathrm{d}q}{\mathrm{d}t}. \tag{41}$$

For sinusoidal base excitation, the magnitude of the response is given as

$$\left|\frac{X}{\omega^2 X_b}\right| = \frac{\sqrt{\alpha^2\Omega^2 + (\beta\Omega^2 - 1)^2}}{\omega_n^2\sqrt{D}}, \tag{42}$$

$$\left|\frac{I}{\omega^2 X_b}\right| = \frac{k_e\sqrt{C_pk\Omega^2}}{\omega_n\sqrt{D}}, \tag{43}$$

$$\left|\frac{P}{\omega^2 X_b}\right| = \frac{k\alpha k_e^2\Omega^2}{\omega_n^3 D}, \tag{44}$$

where,

$$D = \Omega^2(\alpha + 2\zeta + \alpha k_e^2 - (\alpha + 2\beta\zeta)\Omega^2)^2 + (1 - (1 + \beta + 2\alpha\zeta + \beta k_e^2)\Omega^2 + \beta\Omega^4)^2. \tag{45}$$

Again, we cast the same optimization problem with the KKT conditions of Eqs. (12)–(15) with $\mathscr{P}$ given by

$$\mathscr{P} = \frac{k\alpha k_e^2 \Omega^2}{\Omega^2(\alpha + 2\zeta + \alpha k_e^2 - (\alpha + 2\beta\zeta)\Omega^2)^2 + (1 - (1 + \beta + 2\alpha\zeta + \beta k_e^2)\Omega^2 + \beta\Omega^4)^2}. \tag{46}$$

The analysis gives rise to four cases (similar to the analysis in Sections 4 and 5). The results are presented in the following subsection.

6.1. Optimal results for series RL-circuit

The presence of the inductor in series with the resistor leads to the same value of optimal power achieved in Section 5. The optimal power expression obtained here is identical to that of Eq. (36). As such, the results illustrated in Fig. 13a are identical to those shown in Fig. 9a. Similarly, as demonstrated in Figs. 9b and 13b,

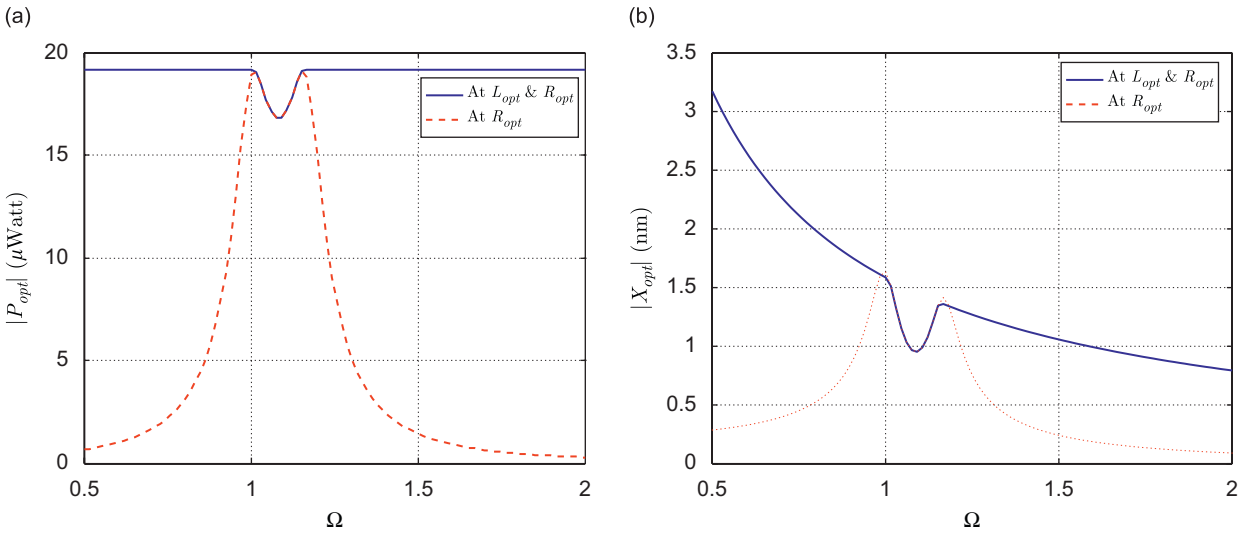

Fig. 13. Optimal power and displacement at $\kappa = 0.6$ and $\zeta = 0.04 < \zeta_b$ (inductor in series): (a) optimal harvested power and (b) optimal displacement.

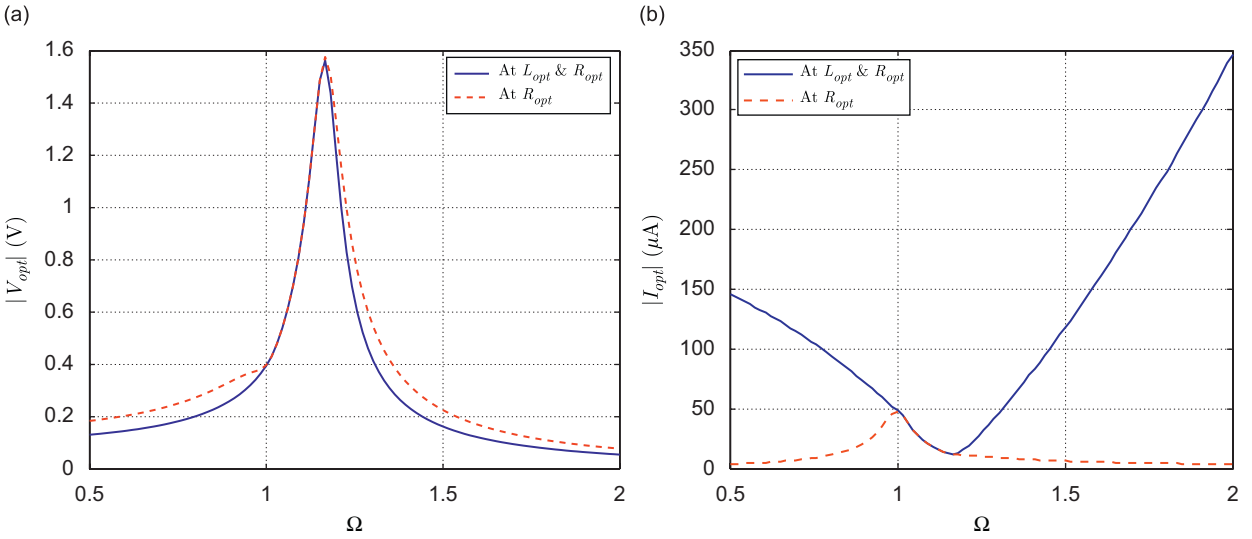

Fig. 14. Optimal voltage and current at $\kappa = 0.6$ and $\zeta = 0.04 < \zeta_b$ (inductor in series): (a) optimal voltage and (b) optimal current.

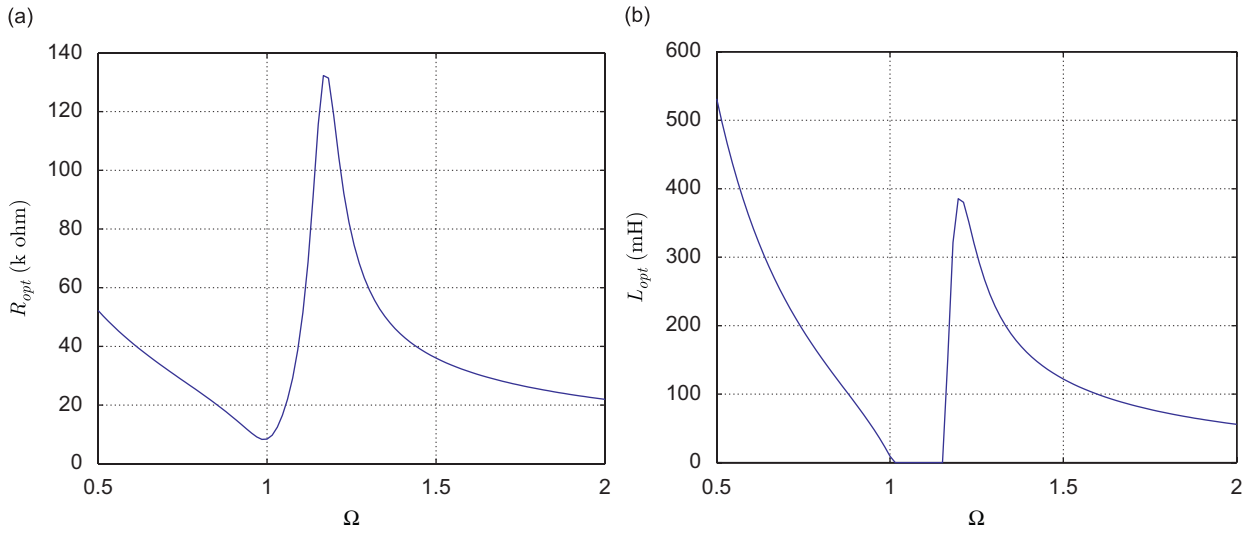

Fig. 15. Optimal resistance and inductance at $\kappa = 0.6$ and $\zeta = 0.04 < \zeta_b$ (inductor in series): (a) optimal resistance and (b) optimal inductance.

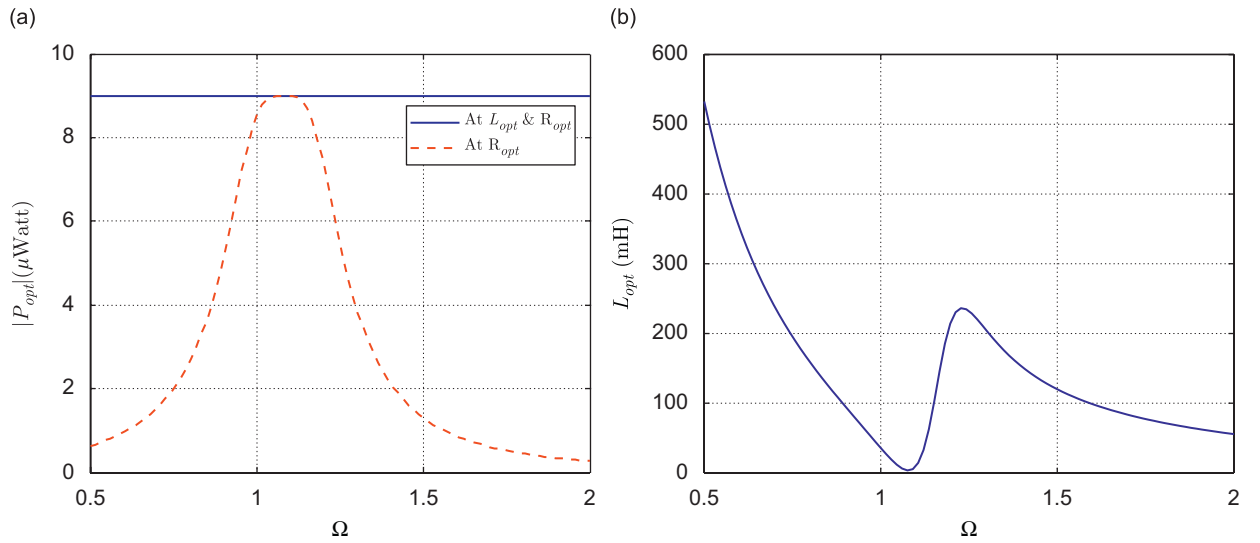

Fig. 16. Optimal harvested power at $\kappa = 0.6$ and $\zeta = 0.085 = \zeta_b$ (inductor in series): (a) optimal harvested power and (b) optimal inductance.

the displacement behavior remains unchanged. Moreover, one would expect that the voltage and current results will change due to the fact that the parallel configuration is a current divider while the series configuration is a voltage divider. Comparing Figs. 10a and 14a, we see that, in general, the magnitude of the voltage is higher for the case of an inductor in parallel. This is reversed for the magnitude of the current when comparing Figs. 10b and 14b. One can conclude that a series connection is more favorable when charging a storage device, which requires high current. However, the parallel configuration is favored when supporting applications that require high voltage such as wireless sensors (Figs. 15–17).

7. Conclusions

In this paper, the optimization problem of a vibration-based energy harvester that utilizes a circuit design consisting of a resistor and an inductor is described. Using the Karush–Kuhn–Tucker (KKT) technique, the

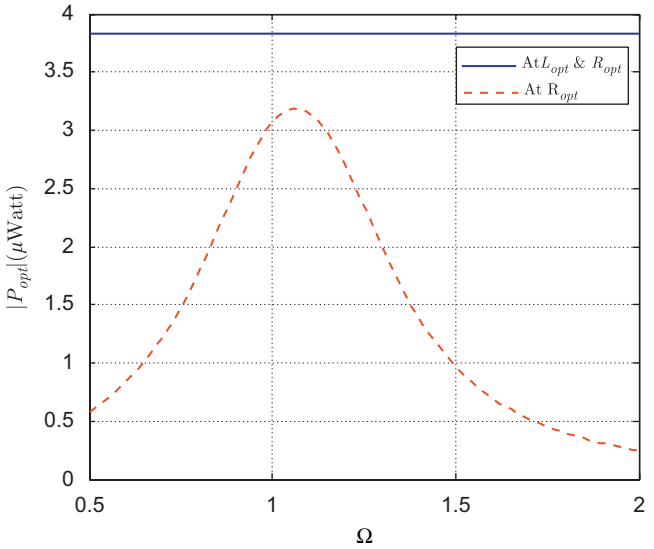

Fig. 17. Optimal power at $\kappa = 0.6$ and $\zeta = 0.2 > \zeta_b$ (inductor in series).

optimization problem is cast as a nonlinear program where the optimal circuit elements are guaranteed to be nonnegative. When treating the resistor-inductor in-parallel and in-series configurations, the optimization problem gives rise to two physically meaningful cases. The first of which suggests utilizing a purely resistive circuit. While this case has received considerable attention in the literature, most of the previous research efforts neglected the effect of mechanical damping on the optimal parameters. In this work, we account for mechanical damping and demonstrate its qualitative effect on power optimality. More specifically, it is shown that for damping ratios that are below a bifurcation damping ratio, the power has two maxima (at the *resonance and antiresonance frequencies*) and one minimum. On the other hand, beyond the bifurcation damping ratio, the power exhibits only one maximum. In addition, we explore the effect of electromechanical coupling on the optimal power and show that materials with higher electromechanical coupling coefficients do not necessarily yield higher output power.

The second case resulting from the optimization problem suggests that by employing an optimal inductor in the circuit, one can substantially enhance the harvested power. In specific, we demonstrate that for damping ratios that are less than the bifurcation damping ratio, one can acquire the maximum power obtained at the resonance and antiresonance frequency for the purely resistive circuit everywhere in the frequency domain except for excitation frequencies between the resonance and antiresonance frequency. On the other hand, when the damping ratio is higher than the bifurcation damping ratio, the harvested power using an inductor can be much higher than that obtained via a purely resistive circuit. The critical implications presented here suggest the following: First, adding an inductor to the circuit allows for tuning the energy harvesting device to scavenge the optimal power for a broad range of excitation frequencies. This implies that it is not necessary to tune the natural frequency of the mechanical element to the resonance or antiresonance frequency to obtain optimal power. Second, in order to maintain optimal power for any excitation frequency it is essential to maintain an optimal strain rate. As such, the power optimization problem is equivalent to optimizing the strain rate of the mechanical element and is not related to the magnitude of the strain itself.

References

[1] H. Sodano, D. Inman, G. Park, A review of power harvesting from vibration using piezoelectric materials, *The Shock and Vibration Digest* 36 (2004) 197–205.

[2] S. Anton, H. Sodano, A review of power harvesting using piezoelectric materials (2003–2006), *Smart Materials and Structures* 16 (2007) 1–21.

[3] H. Sodano, D. Inman, G. Park, Generation and storage of electricity from power harvesting devices, *Journal of Intelligent Material Systems and Structures* 16 (2005) 67–75.
[4] H. Sodano, D. Inman, G. Park, Comparison of piezoelectric energy harvesting devices for recharging batteries, *Journal of Intelligent Material Systems and Structures* 16 (2005) 799–807.
[5] B. Grisso, D. Inman, Towards autonomous sensing, in: M. Tomizuka (Ed.), *Smart Structures and Materials*: *Sensors and Smart Structures Technologies for Civil*, *Mechanical and Aerospace Systems*, *Vol. 6174 of Proceedings of SPIE*, San Diego, CA, 2006, pp. 248–254.
[6] J. Rastegar, C. Pereira, H.-L. Nguyen, Piezoelectric-based power sources for harvesting energy from platforms with low frequency vibration, in: E. White (Ed.), *Smart Structures and Materials*: *Damping and Isolation*, *Vol. 6171 of Proceedings of SPIE*, San Diego, CA, 2006, pp. 1–7.
[7] S. Priya, D. Popa, F. Lewis, Energy efficient mobile wireless sensor networks, *Proceedings of ASME International Mechanical Engineering Congress & Exposition*, Chicago, IL, 2006, paper number IMECE2006-14078, 8pp.
[8] E. Lefeuvre, A. Badel, C. Richard, L. Petit, D. Guyomar, A comparison between several vibration-powered piezoelectric generators for standalone systems, *Sensors and Actuators* 126 (2006) 405–416.
[9] A. Badel, D. Guyomar, E. Lefeuvre, C. Richard, Piezoelectric energy harvesting using a synchronized switch technique, *Journal of Intelligent Material Systems and Structures* 17 (2006) 831–839.
[10] T. Anderson, D. Sexton, A vibration energy harvesting sensor platform for increased industrial efficiency, in: M. Tomizuka (Ed.), *Smart Structures and Materials*: *Sensors and Smart Structures Technologies for Civil*, *Mechanical and Aerospace Systems*, *Vol. 6174 of Proceedings of SPIE*, San Diego, CA, 2006, pp. 621–629.
[11] S. Roundy, On the effectiveness of vibration-based energy harvesting, *Journal of Intelligent Material Systems and Structures* 16 (2005) 425–808.
[12] N. Stephen, On energy harvesting from ambient vibration, *Journal of Sound and Vibration* 293 (1) (2006) 409–425.
[13] N. duToit, B. Wardle, S.-G. Kim, Design considerations for mems-scale piezoelectric mechanical vibration energy harvesters, *Integrated Ferroelectrics* 71 (2005) 121–160.
[14] W.-J. Wu, Y.-Y. Chen, B.-S. Lee, J.-J. He, Y.-T. Pen, Tunable resonant frequency power harvesting devices, in: W. Clark, M. Ahmadian, A. Lumsdaine (Eds.), *Smart Structures and Materials*: *Damping and Isolation*, *Vol. 6169 of Proceedings of SPIE*, San Diego, CA, 2006, p. 61690A.
[15] J. Twiefel, B. Richter, T. Hemsel, Wallaschek, Model based design of piezoelectric energy harvesting systems, in: W. Clark, M. Ahmadian, A. Lumsdaine (Eds.), *Smart Structures and Materials*: *Damping and Isolation*, *Vol. 6169 of Proceedings of SPIE*, San Diego, CA, 2006, p. 616909.
[16] T. Johnson, D. Charnegie, W. Clark, M. Buric, G. Kusic, Energy harvesting from mechanical vibrations using piezoelectric cantilever beams, in: W. Clark, M. Ahmadian, A. Lumsdaine (Eds.), *Smart Structures and Materials*: *Damping and Isolation*, *Vol. 6169 of Proceedings of SPIE*, San Diego, CA, 2006, pp. 81–92.
[17] N. duToit, B. Wardle, Experimental verification of models for microfabricated piezoelectric energy harvesters, *AIAA Journal* 45 (5) (2007) 1126–1137.
[18] K. Nakano, S.J. Elliott, E. Rustighi, A unified approach to optimal conditions of power harvesting using electromagnetic and piezoelectric transducers, *Smart Materials and Structures* 16 (2007) 948–958.
[19] G. Lesieutre, G. Ottman, H. Hofmann, Damping as a result of piezoelectric energy harvesting, *Journal of Sound and Vibration* 269 (2004) 991–1001.
[20] W.L. Winston, *Operations Research: Applications and Algorithms*, fourth ed., Duxbury Press, Pacific Grove, CA, 2003.
[21] A. Erturk, D. Inman, A distributed parameter electromechanical model for cantilevered piezoelectric energy harvesters, *Journal of Vibration and Acoustics*, *Transaction of ASME* 13 (4) (2008) 1–15.
[22] A. Erturk, D. Inman, On mechanical modeling of cantilevered piezoelectric vibration energy harvesters, *Journal of Intelligent Material Systems and Structures*, doi:10.1177/1045389X07085639, to appear April (2008).
[23] R. Sood, Piezoelectric Micro Power Generator (PMPG): a MEMS-based Energy Scavenger, Master's Thesis, Massachusets Institute of Technology, Cambridge, MA, May 2003.
[24] G. Lesieutre, C. Davis, Can a coupling coefficient of a piezoelectric device be higher than those of its active material?, *Journal of Intelligent Material Systems and Structures* 8 (1997) 859–867.